Review Article

Eugene Oks*, Elisabeth Dalimier, Paulo Angelo, and Tatiana Pikuz

Review of recent analytical advances in the spectroscopy of hydrogenic lines in plasmas

https://doi.org/10.1515/phys-2024-0002
received November 14, 2023; accepted March 06, 2024

Abstract: Broadening of hydrogenic spectral lines is an important tool in spectroscopic diagnostics of various laboratory and astrophysical plasmas. We review recent analytical advances in three areas. First, we review the analytical solution for the splitting of hydrogenic lines under the combination of a circularly polarized electromagnetic wave with a strong magnetic field. Practical applications of this solution relate to the spectroscopic diagnostic of the electron cyclotron waves and to the relativistic laser–plasma interactions. Second, we review analytical results concerning the Stark–Zeeman broadening of the Lyman-alpha (Ly-alpha) line in plasmas. These results allow for the Stark width of the Ly-alpha π-component to be used for the experimental determination of the ion density or of the root-mean-square field of a low-frequency electrostatic plasma turbulence in the situation where the Zeeman effect dominates over the Stark effects. Third, we review recent analytical advances in the area of the intra-Stark spectroscopy: three different new methods, based on the emergent phenomenon of the Langmuir-wave-caused structures ("L-dips") in the line profiles, for measuring super-strong magnetic fields of the GigaGauss range developing during relativistic laser–plasma interactions. We also review the rich physics behind the L-dips phenomenon – because there was a confusion in the literature in this regard.

Keywords: broadening of hydrogenic spectral lines in plasmas, strong magnetic field, intra-Stark spectroscopy, Langmuir-wave-caused structures, relativistic laser, plasma interactions, electron cyclotron waves

*** Corresponding author: Eugene Oks**, Physics Department, Auburn University, 380 Duncan Drive Auburn, AL 36849, United States of America, e-mail: oksevgu@auburn.edu
Elisabeth Dalimier, Paulo Angelo: LULI - Sorbonne Université, CNRS, Ecole Polytechnique, CEA: Université Paris-Saclay, F-75252 Paris cedex 05, France
Tatiana Pikuz: Open and Transdisciplinary Research Initiatives, Osaka University, Osaka 565-0871, Japan

1 Introduction

Spectroscopic diagnostics of various laboratory and astrophysical plasmas employ the broadening of spectral lines as an important tool – see, *e.g.*, books published in the last three decades [1–7] (listed in the reverse chronological order) and references therein. Hydrogenic spectral lines are especially sensitive for providing the diagnostic information about various fields inside plasmas.

We focus on the analytical advances for the following reasons. First, analytical results provide the physical insight on the phenomena under consideration – in distinction to simulations. Second, analytical results can capture emergent phenomena – in distinction to simulations: see, *e.g.*, the illuminating study by Post and Votta [8] providing, in particular, examples of failures of major codes due to the inadequate verification and validation.

In Section 2, we review the results from the study by Oks *et al.* [9] where the authors obtained an analytical solution for the splitting of hydrogenic spectral lines under the combination of a circularly polarized electromagnetic wave with a strong magnetic field. It turned out to be possible to decrease the splitting of hydrogenic spectral lines by changing the magnetic field. This was a *counterintuitive* result. Moreover, it was also found that at the value of the magnetic field, achieving the absolute minimum of the splitting, the total intensity of the spectral line decreases by 40%. This was yet another *counterintuitive* result. In the study by Oks *et al.* [9], two possible practical applications of these counterintuitive results were listed. The first application relates to the spectroscopic diagnostic of the electron cyclotron waves used as an additional heating method for plasmas in magnetic fusion machines. The second application relates to relativistic laser plasma interactions.

In Section 3, we review the results from the study by Oks [10] where the author obtained analytical results for the Stark–Zeeman broadening of the Lyman-alpha (Ly-alpha) line in plasmas. The emphasis was on the π-component of the Ly-alpha line – the component having the most remarkable, practically important properties.

Previously, it was found that under the conditions typical for the edge plasmas of tokamaks, the Stark width of the Ly-alpha π-component can be used for the experimental determination of the effective charge of ions, while the Ly-alpha σ-component or any component of any other hydrogenic spectral line cannot be used for this purpose [11]. It was also found previously that the Stark width of the Ly-alpha π-component, emitted by atoms of the hydrogen or deuterium neutral beam injected for heating tokamak plasmas, can be employed for the simultaneous experimental determination of both the effective charge of ions and of the pitch angle (the angle between the beam velocity and the magnetic field) [12]. Oks [10] demonstrated another remarkable property of the Ly-alpha π-component. Namely, in the situation where the Zeeman effect dominates over the Stark effects, the broadening of the Ly-alpha π-component turned out to be controlled by the linear Stark effect – while this was not the case for the Ly-alpha σ-component or any component of any other hydrogenic spectral line. Therefore, the Stark width of the Ly-alpha π-component can be used in this situation for the experimental determination of the ion density or of the root-mean-square field of a low-frequency electrostatic plasma turbulence (LEPT), such as ion-acoustic waves, Bernstein modes, or low-hybrid waves.

In Section 4, we review the latest analytical results on the intra-Stark spectroscopy (ISS). The ISS is the spectroscopy within the quasistatic Stark profile of a spectral line. For the first time, the term ISS was introduced in previous studies [13,14]. This was due to a physical similarity with the well-known intra-Doppler spectroscopy, where because of nonlinear optical phenomena some depressions appear at certain position within the Doppler profile of a spectral line. In the ISS, some local depressions ("dips") appear at certain positions within the quasistatic Stark profile of a spectral line. This phenomenon relates to the situation where radiating atoms/ions are subjected to a quasistatic field $\mathbf{F}$ and to a quasimonochromatic electric field $\mathbf{E}(t)$ at the characteristic frequency ω and to a quasistatic field $\mathbf{F}$, simultaneously. The underlying physical reason for this phenomenon is the dynamic resonance between the Stark splitting of hydrogenic spectral lines and the frequency ω or its harmonics. The most important difference between the ISS and the intra-Doppler spectroscopy is that in the ISS, despite the fact that the applied electric field is quasimonochromatic, there arises a nonlinear dynamic resonance of a multifrequency nature, as explained in detail by Gavrilenko and Oks [15]. More theoretical details on the ISS can be found in the study by Oks [7].

In the relevant experimental research, most studies dealt with the case where the dynamic field $\mathbf{E}(t)$ was represented by a Langmuir wave. The standard terminology became to call the corresponding structures/modulations in spectral line profiles as the L-dips – though these localized structures can consist of the primary minimum ("the dip") and two surrounding bumps.

Studies of the L-dips are practically important for three reasons. First, they allow measuring the electron density N_e in plasmas more accurately than, *e.g.*, the value of N_e deduced from the line broadening measurements. The benchmark experiment of Kunze's group [14] (the experiment where plasma parameters were determined independently, not based on the spectral line shapes) demonstrated that the L-dip-based passive spectroscopic method yields the same

high accuracy as the active spectroscopic method employing the Thompson scattering (the latter being more complex experimentally). Second, they furnish the sole non-perturbative method for the experimental determination of the Langmuir waves amplitude in plasmas. Third, they reveal the rich physics of laser–plasma interaction – especially in the case of the relativistic laser–plasma interaction. The study by Oks [7] and later reviews [16–18] epitomize the experimental research on the L-dips as applied to spectroscopic diagnostics of various plasmas.

So, in Section 4, we review the recent theoretical additions to the ISS published in previous studies [19–21]. In these works, the authors proposed three different methods, based on the ISS, for measuring ultra-strong magnetic fields of the GigaGauss or even multi-GigaGauss range developing at the surface of the relativistic critical density (according to, *e.g.*, review by Belyaev *et al.* [22] and previous studies [23–31]) during relativistic laser–plasma interactions.

2 Magnetic-field-caused narrowing of hydrogenic spectral lines under a circularly polarized electromagnetic wave

Lisitsa [32] presented an exact analytical solution for the splitting of hydrogen lines under the electric field $\mathbf{F}_0$ that rotates with the angular velocity $\mathbf{\Omega}$, the magnitude of the angular velocity being constant. After proceeding to the reference frame that rotated with the same angular velocity as the field, the situation got simplified to a hydrogen atom in the crossed fields, namely, in the static electric field perpendicular to a fictitious static magnetic field $\mathbf{B}_{\text{fict}} = -2m_e c\mathbf{\Omega}/e$. The latter problem had a known

analytical solution presented by Demkov *et al.* [33]. Physically, this simplification became possible as the consequence of the O_4 symmetry of hydrogen atoms revealed by Fock [34][1].

Oks *et al.* [9] added to the above system a true magnetic field **B** that was considered to be parallel or antiparallel to the vector **Ω**. Then, the interaction term became

$$V = \mathbf{erF}_0 + \mu_B \mathbf{LB}_{\text{eff}}, \tag{1}$$

where the effective magnetic field was

$$\mathbf{B}_{\text{eff}} = \mathbf{B}_{\text{fict}} + \mathbf{B}, \tag{2}$$

while **r** and **L** were the operators of the position vector and the angular momentum, respectively (**L** being in units of $\hbar$); μ_B is the Bohr magneton. Figure 1 shows the possible mutual orientations of the three vectors entering Eq. (2).

The situation became mathematically equivalent to the hydrogenic atom or ion under a circularly polarized wave, in which the electric field rotates with the following effective angular velocity

$$\mathbf{\Omega}_{\text{eff}} = -(\mu_B/\hbar)(\mathbf{B}_{\text{fict}} + \mathbf{B}) = \mathbf{\Omega} - \mu_B\mathbf{B}/\hbar. \tag{3}$$

Then, in the study by Oks *et al.* [9], the following quantities were defined:

$$\mathbf{N} = \hbar n\mathbf{A}/Z, \quad \mathbf{A} = (\mathbf{p}x\mathbf{L} - \mathbf{L}x\mathbf{p})/(m_e e^2) - Zr/r. \tag{4}$$

where **A** is the dimensionless Runge–Lenz vector, n is the principal quantum number of the state of the hydrogenic atom or ion with the nuclear charge Z, and **p** is the linear momentum. Then, the following vectors were introduced by Oks *et al.* [9]:

$$\mathbf{J}_i = [\hbar\mathbf{L} + (-1)^i\mathbf{N}]/2, \quad \mathbf{\omega}_i = \mathbf{\Omega}_{\text{eff}} + (-1)^i\mathbf{\Omega}_F, \quad i = 1, 2. \tag{5}$$

where

$$\mathbf{\Omega}_F(n) = -[3n\hbar/(2Zm_e e)]\mathbf{F}_0. \tag{6}$$

Thereafter, Eq. (1) was reformulated as

$$V = -\mathbf{J}_1\mathbf{\omega}_1 - \mathbf{J}_2\mathbf{\omega}_2. \tag{7}$$

The corresponding Hamiltonian was then diagonalized on the basis of the Demkov-Monozon-Ostrovsky wave functions $u_{nn'n''}$ [33]. These wave functions correspond to the definite projection of vector $\mathbf{J}_1$ on vector $\mathbf{\omega}_1$, controlled by the quantum number n', and to the definite projection of vector $\mathbf{J}_2$ on vector $\mathbf{\omega}_2$, controlled by the quantum number n''. These quantum numbers n' and n'' take the following set of values: $-(n-1)/2$, $-(n-1)/2+1$, $-(n-1)/2+2$, ..., $(n-1)/2$. The energy levels of this quantum system were as follows:

$$E_{nn'n''} = -m_e Z^2 e^4/(2n^2\hbar^2) - (n' + n'')\omega. \tag{8}$$

where

$$\begin{aligned}\omega &= |\omega_1| = |\omega_2| \\ &= \{[\Omega - (\mu_B B/\hbar)\text{sign}(\mathbf{B\Omega})]^2 + 9n^2\hbar^2F_0^2/(4Z^2m_e^2e^2)\}^{1/2}.\end{aligned} \tag{9}$$

In the rotating reference frame, the eigenfunctions had the following form:

$$\chi = u_{nn'n''} \exp[-i\omega_0 t + i\omega t(\text{ni}' + \text{ni}'' - \text{nf}' - \text{nf}'')] \tag{10}$$

where ni′ and ni″ denote the quantum numbers n' and n'' of the initial sublevel engaged in the radiative transition; nf′ and nf″ denote the quantum numbers n' and n'' of the final sublevel engaged in the radiative transition; ω_0 is the unperturbed frequency of the spectral line under consideration.

The spectral line profile $S(\omega)$ was presented as follows:

$$\begin{aligned}S(\omega) = &\sum_{\text{ni}',\ \text{ni}'',\ \text{nf}',\ \text{nf}''} \sum_{l=0,\ \pm1} \Bigg| \sum_{\text{ki1},\ \text{ki2},\ \text{kf1},\ \text{kf2}} D_{\text{ni}',\ \text{ki}}^{(\text{ni}-1/2)}(0,\ \alpha_1^i,\ \\ &\times 0) D_{\text{ni}'',\ \text{ki2}}^{(\text{ni}-1/2)}(0,\ \alpha_2^i,\ 0) \\ &D_{\text{nf}'\text{kf1}}^{(\text{nf}-1/2)}(0,\ \alpha_1^f,\ 0) D_{\text{nf}''\text{kf2}}^{(\text{nf}-1/2)}(0,\ \alpha_2^f,\ 0) \\ &\langle \text{ni},\ \text{ki1},\ \text{ki2}|d_l|\text{nf},\ \text{kf1},\ \text{kf2}|\rangle|^2 \delta(\Delta\omega - \Delta\omega_{\text{if}} + l\Omega)\end{aligned} \tag{11}$$

where

$$\Delta\omega_{\text{if}} = \omega(\text{ni}' + \text{ni}'' - \text{nf}' - \text{nf}'') \tag{12}$$

Also, in Eq. (11), $D_{\text{mm}'}^{(j)}(\varphi_1, \theta, \varphi_2)$ are the D-functions defined by Wigner [38]. As for d_l, they are the spherical components of the electric dipole moment in Wigner definition [38] – *e.g.*,:

$$2^{1/2}d_{-1} = d_x + id_y = -2^{1/2}d_{+1}. \tag{13}$$

The matrix elements of d_l were calculated on the basis of the parabolic wave functions $|n\ k1\ k2\rangle$ with the symmetry axis along $\mathbf{F}_0$. The second arguments of the D-functions in Eq. (11) are the following angles:

$$\begin{aligned}\alpha_2^i &= \arctan[\Omega_{\text{eff}}/\Omega_F(\text{ni})], \quad \alpha_1^i = \pi - \alpha_2^i, \\ \alpha_2^f &= \arctan[\Omega_{\text{eff}}/\Omega_F(\text{nf})], \quad \alpha_1^f = \pi - \alpha_2^f.\end{aligned} \tag{14}$$

The analytical solution given above shows that the spectral line splits into components such that their separation from each other is equal either to the quantity ω from Eq. (9) or to the electric field frequency Ω. The dominating outcome is the separation by the quantity ω controlled by the electric field amplitude F_0 and frequency Ω, as well as

1 We note in passing that the idea of proceeding to the reference frame rotated with the same angular velocity as the electric field was later used for finding exact analytical solutions for the Stark broadening of hydrogen lines [35] or hydrogen-like lines [36] in plasmas, as well as for the Stark broadening of helium or helium-like lines [37].

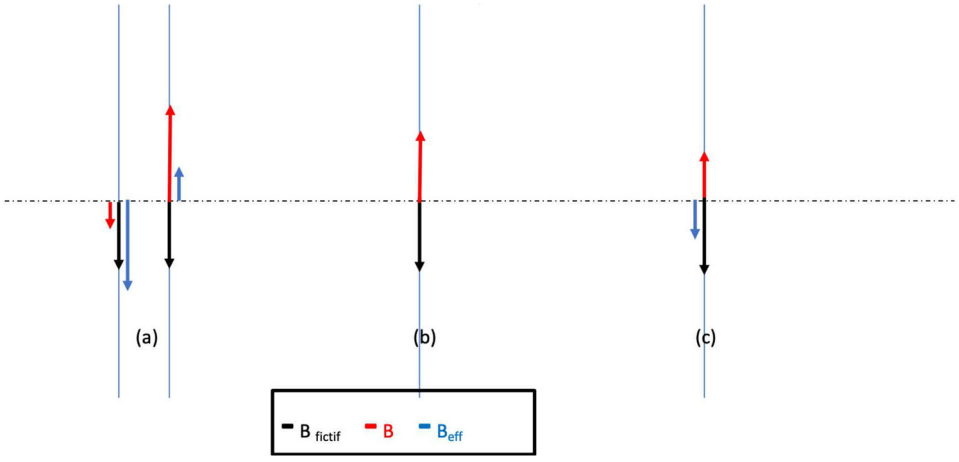

Figure 1: Possible mutual orientations of the three vectors entering Eq. (2): (a) $\mathbf{B}_{\rm eff}$ is in the same direction as **B**; (b) $\mathbf{B}_{\rm eff}$ is zero; and (c) $\mathbf{B}_{\rm eff}$ is in the opposite direction compared to **B**.

by the true magnetic field B. It is easy to see from Eq. (9) that the separation between the spectral line components *decreases* if the true magnetic field **B** is parallel to **Ω** (and thus antiparallel to the fictitious magnetic field $\mathbf{B}_{\rm fict} = -\hbar\mathbf{\Omega}/\mu_{\rm B}$). This is a *counterintuitive* result.

In the situation where the true magnetic field **B**, being parallel to **Ω**, has the absolute value

$$B = 2m_{\rm e}c\Omega/e, \tag{15}$$

the dominating separation between the spectral line components diminishes to $3n\hbar F_0/(2Zm_{\rm e}e)$. This means that by the corresponding choice of the true magnetic field, the dominating separation between the components of the spectral line takes the minimum possible value – the value being just the Stark splitting.

We use the Ly-alpha line to illustrate the general analytical solution. Figure 2 shows the calculated profiles of the Ly-alpha line *vs* the scaled detuning $\Delta\omega/\Omega$ from the line center for three different values of the following parameter:

$$q_{\rm eff} = [3n\hbar/(2Zm_{\rm e}e)]F_0/\Omega_{\rm eff}, \tag{16}$$

namely, for $q_{\rm eff} = 1$ (solid line), $q_{\rm eff} = 4$ (dashed line), and $q_{\rm eff} = 7$ (dash-dotted line). The profiles were calculated based on the analytical results for the frequencies and intensities given in Table 1 in the study by Oks [37] by substituting Ω by $\Omega_{\rm eff}$ and the parameter $q = [3nh/(2Zm_{\rm e}e)]F_0/\Omega$ by $q_{\rm eff}$. It is seen that as the parameter $q_{\rm eff}$ increases, most line components move away from the line center and all seven line components become more clearly visible.

Oks *et al.* [9] also showed that in the situation where the fictitious magnetic field gets completely canceled out by the true magnetic field (*i.e.*, $\mathbf{B} = -\mathbf{B}_{\rm fict}$), the total intensity of the Ly-alpha line decreases by 40%. This is yet another *counterintuitive* result.

Possible practical applications of the above counterintuitive results relate to the spectroscopic diagnostic of the electron cyclotron waves in magnetic fusion plasmas, as well as to relativistic laser–plasma interactions (as noted in Section 1).

3 Stark–Zeeman broadening of the Ly-alpha line in plasmas

The broadening of spectral lines in magnetized plasmas was studied in a number of papers, as summarized, *e.g.*,

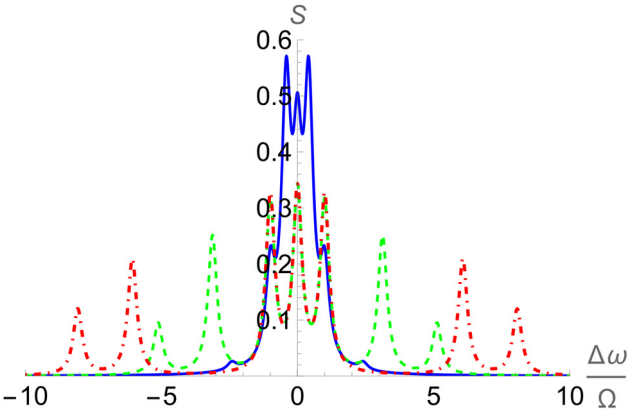

Figure 2: Calculated profiles of the Ly-alpha line *vs* the scaled detuning $\Delta\omega/\Omega$ from the line center for three different values of the following parameter $q_{\rm eff} = [3n\hbar/(2Zm_{\rm e}e)]F_0/\Omega_{\rm eff}$: for $q_{\rm eff} = 1$ (solid line), $q_{\rm eff} = 4$ (dashed line), and $q_{\rm eff} = 7$ (dash-dotted line). Each line component was assigned the Lorentzian shape of the full width at half maximum (FWHM) equal to 0.4 Ω representing other broadening mechanisms, such as the Doppler broadening.

in books (referred here in the reversed chronological order) [2,3,5,6,39,40]. In this section, we focus on the π-component of the Ly-alpha line of hydrogenic atoms because it has the most remarkable, practically important properties. In the study by Derevianko and Oks [11], by using an advanced analytical theory, it was demonstrated that for the edge plasmas of tokamaks, the Stark width of the Ly-alpha π-component can be used for the experimental determination of the effective charge of ions, while the Ly-alpha σ-component or any component of any other hydrogenic spectral line cannot be used for this purpose. Derevianko and Oks [12], by using the same advanced analytical theory as in their previous study [11], showed that the Stark width of the Ly-alpha π-component, emitted by atoms of the hydrogen or deuterium neutral beam injected for heating tokamak plasmas, can be utilized for determining experimentally both the effective charge of ions and the angle between the beam velocity and the magnetic field (the pitch angle), as noted in Section 1.

In the study by Oks [10], another significant feature of the Ly-alpha π-component was demonstrated. In the case where the Zeeman effect is stronger than the Stark effect, the broadening of the Ly-alpha π-component turned out to be controlled by the linear Stark effect, practically without depending on the magnetic field – in distinction to the Ly-alpha σ-component or any component of any other hydrogenic spectral line. Therefore, the Stark width of the Ly-alpha π-component can be utilized in these conditions for determining experimentally the ion density or of the root-mean-square field of a LEPT, such as ion-acoustic waves, Bernstein modes, or lower-hybrid waves, as noted in Section 1. Below are some details.

In the study by Oks [10], there was considered the splitting/broadening of the Ly-alpha line of a hydrogenic atom of the nuclear charge Z under a magnetic field **B** (the direction of which we choose as the z-axis) and an electric field **F** at the angle θ with respect to **B**. We use atomic units: $\hbar = m_e = e = 1$. For the absolute values of these fields, we introduce the following scaled notations:

$$M = \alpha B/2, \quad E = 3F/Z. \tag{17}$$

where α is the fine structure constant; "M" stands for the "magnetic"; and "E" stands for "electric." Then, the matrix elements of the interaction term in the Hamiltonian can be represented in the form (see, *e.g.*, [41]):

0	0	E	0
0	$-M\cos\theta$	$2^{-1/2}M\sin\theta$	0
E	$2^{-1/2}M\sin\theta$	0	$2^{-1/2}M\sin\theta$
0	0	$2^{-1/2}M\sin\theta$	$M\cos\theta$

The eigenvalues of this matrix satisfy the following equation:

$$(\Delta\omega)^2 = (E^2 + M^2)/2 \pm [(E^2 + M^2)^{2/4} - E^2M^2\cos^2\theta]^{1/2}. \tag{18}$$

(It should be reminded that in atomic units, the splitting has the same expression both in terms of the energy and in terms of the frequency.)

In the case where the electric field dominates, *i.e.*, $E \gg M$, Eq. (18) yields

$$\Delta\omega \approx \pm M\cos\theta. \tag{19}$$

for the σ-component and

$$\Delta\omega \approx \pm[E + (M^2\sin^2\theta)/(2E]. \tag{20}$$

for the π-component.

In the opposite case where the magnetic field dominates, *i.e.*, $E \ll M$, Eq. (18) yields

$$\Delta\omega \approx \pm[B + (E^2\sin^2\theta)/(2B]. \tag{21}$$

for the σ-component and

$$\Delta\omega \approx \pm E\cos\theta, \tag{22}$$

for the π-component.

Usually, the value and the direction of the magnetic field in a plasma is known. As for the electric field E, it can be represented by the LEPT and/or by the quasistatic part of the ion microfield. Therefore, the most interesting situation is posed *via* Eq. (22): despite the magnetic field dominating, the splitting/broadening of the π-component is linear with respect to the projection of the electric field on the direction of the magnetic field. This is a *counter-intuitive* result. Thus, the Stark broadening of the π-component (that we calculate analytically below) offers the opportunity for the experimental determination of either the root-mean-square field F_t of the LEPT or of the ion density in strongly magnetized plasmas, as detailed at the end of this section.

The Stark profile of the π-component at the fixed absolute value of the electric field is obtained by averaging over the spherically symmetric angular distribution as follows:

$$S(\Delta\omega, E) = \int_0^1 d(\cos\theta)\delta(|\Delta\omega| - E\cos\theta) = (1/E)\Theta(E - |\Delta\omega|). \tag{23}$$

where $\delta(...)$ is the delta-function and $\Theta(...)$ is the theta-function.

The next step is the averaging over the distribution of the absolute value of the LEPT, given by the Rayleigh distribution [2,42,43]. The latter is

$$W(f)\mathrm{d}f = 3(6/\pi)^{1/2}f^2\exp(-3f^2/2)\mathrm{d}f, \quad f = F/F_t, \tag{24}$$

where F_t is the root-mean-square field of the LEPT for the distribution $W(f)\mathrm{d}f$.

Since

$$1/E = Z/(3F) = Z/(3F_t f), \tag{25}$$

then the Stark profile of the π-component becomes

$$S(\Delta\omega) = [Z/(3F_t)] \int_{f_{min}}^{\infty} \mathrm{d}f W(f)/f, \quad f_{min}(\Delta\omega) = Z|\Delta\omega|/(3F_t). \tag{26}$$

The appearance of $f_{min}(\Delta\omega)$ is due to the restriction that the absolute value of $\cos\theta$ in the argument of the delta-function in Eq. (23) cannot exceed unity.

After calculating the integral, in the study by Oks [10], the following final expression was obtained for the Stark profile of the π-component:

$$S(\Delta\omega) = [Z/(3F_t)](6/\pi)^{1/2} \exp\{-3[f_{min}(\Delta\omega)]^2/2\}. \tag{27}$$

Figure 3 displays the scaled Stark profile

$$s(D) = 3F_t S(D)/Z. \tag{28}$$

vs the scaled detuning

$$D = Z\Delta\omega/(3F_t). \tag{29}$$

The FWHM of the above Stark profile is 1.36 in terms of the scaled detuning D or 4.08 F_t/Z in terms of $\Delta\omega$. Thus, by measuring the experimental FWHM of the Ly-alpha π-component, one can determine the root-mean-square field F_t of the LEPT in strongly magnetized plasmas.

The distribution $W(f)\mathrm{d}f$ from Eq. (24) describes the isotropic LEPT. This is relevant to the late stage of the development of the LEPT. At the early stage, the LEPT can be anisotropic. For example, it can have the shape of a very oblate spheroid. This situation is relevant to the Berstein modes (*e.g.*, [44–46]). The distribution is practically two-dimensional, as follows (*e.g.*, [2]):

$$W_2(f)\mathrm{d}f = 2f \exp(-f^2)\mathrm{d}f, \quad f = F/F_t, \tag{30}$$

where F_t is the root-mean-square field of the LEPT for the distribution $W_2(f)\mathrm{d}f$.

The corresponding Stark profile of the π-component can be calculated using Eq. (26) on the substitution of $W(f)$ by $W_2(f)$, yielding the following:

$$S(\Delta\omega) = [Z/(3F_t]\pi^{1/2}\mathrm{Erfc}[f_{min}(\Delta\omega)], \tag{31}$$

where Erfc[...] is the complementary error function and $f_{min}(\Delta\omega)$ is already defined in Eq. (26).

Figure 4 displays the corresponding scaled Stark profile $s(D)$ *vs* the scaled detuning D, where $s(D)$ and D were defined in Eqs. (28) and (29), respectively. It is seen that the profile has the cusp in the center, which is a quite rare shape of the Stark profile of a spectral line (or its component) in plasmas.

Further, in the study by Oks [10], there was provided a model example for the situation where the electric field is represented by the quasistatic part of the ion microfield. The averaging of the profile $S(\Delta\omega, E)$ from Eq. (23) was performed over the binary distribution of the ion microfield. The latter distribution corresponds to the following distribution of the distance R of the nearest neighbor ion from the radiating atom:

$$P(r)\mathrm{d}r = 3r^2 \exp(-r^3), \quad r = R/R_0, \tag{32}$$

where the mean interionic distance is

$$R_0 = [3/(4\pi N_i)]^{1/3}, \tag{33}$$

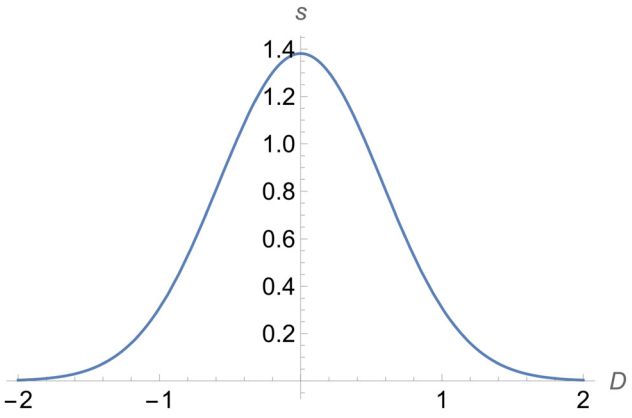

Figure 3: The scaled Stark profile $s(D)$ of the Ly-alpha π-component (given by Eq. (28)) *vs* the scaled detuning D (given by Eq. (29)) for the situation where the scaled electric field E (represented by a LEPT) is much smaller than the magnetic field M (both fields are defined in Eq. (17)) [10].

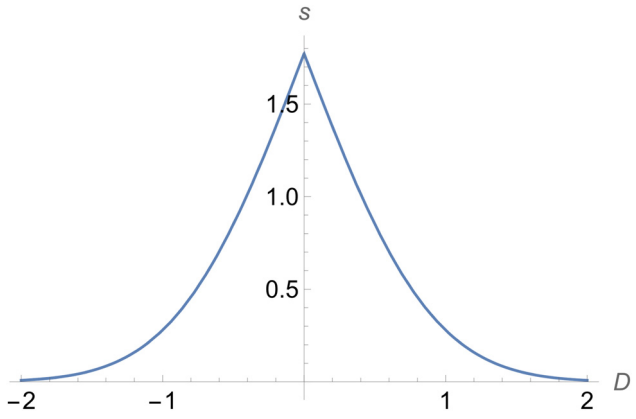

Figure 4: Same as in Figure 3, but for the two-dimensional distribution of the LEPT.

where N_i is the ion density. The relation between E and r is given as follows:

$$1/E = ZR_0^2 r^2/(3Z_i), \tag{34}$$

where Z_i is the charge of the perturbing ions. Then, the averaging can be expressed as

$$\begin{aligned} S(\Delta\omega) &= (ZR_0^2/Z_i)\int_0^{r_{\max}} \mathrm{d}r \;\; r^4 \exp(-r^3) \\ &= [ZR_0^2/(3Z_i)]\{\Gamma(5/3) \\ &\quad - [r_{\max}(\Delta\omega)]^5 \, \varphi_{2/3}[(r_{\max}(\Delta\omega))^3]\}, \end{aligned} \tag{35}$$

where $\Gamma(5/3)$ is the gamma function, $\varphi_{2/3}(r_{\max}{}^3)$ is the Misra function (which is equal to the exponential integral function of the same argument, but of the negative index –2/3), and

$$r_{\max}(\Delta\omega) = 3Z_i/(ZR_0^2|\Delta\omega|). \tag{36}$$

The appearance of $r_{\max}(\Delta\omega)$ is due to the fact that according to Eq. (34), r is inversely proportional to the square root of F. Since the value of $f = F/F_t$ is limited from below (*e.g.*, Eq. (26)), then the value of r is limited from above.

Figure 5 displays the corresponding scaled Stark profile

$$s(D) = 3Z_i S(D)/(ZR_0^2). \tag{37}$$

vs the scaled detuning

$$D = ZR_0^2|\Delta\omega|/(3Z_i). \tag{38}$$

(We note again that the definition of $s(D)$ and D in Eqs. (37) and (38) differ from the analogous notations from Eqs. (28) and (29).)

It is seen that the Stark profile of the Ly-alpha π-component has a unique feature: the flat top. This is a *counter-intuitive* result: among the garden variety of Stark profiles of hydrogenic spectral lines previously presented in the vast amount of the literature on the Stark broadening, the flat top profile was never encountered previously.

The FWHM of the above Stark profile is 1.64 in terms of the scaled detuning D or $4.92Z_i/(ZR_0{}^2)$ in terms of $\Delta\omega$. We note that the latter FWHM is proportional to $N_i^{2/3}$ – according to the definition of R_0 from Eq. (44). Thus, by measuring the experimental FWHM of the Ly-alpha π-component in this situation, one can determine the ion density (and therefore, the electron density) in strongly magnetized plasmas.

Of course, the latest of the above examples is based on a relatively simple model. The corresponding results for a more sophisticated model will be published elsewhere.

Thus, the π-component of the Ly-alpha line has indeed unique properties. This is a clear distinction of the π-component of the Ly-alpha line from the σ-component of this line or from any component of any other hydrogen line.

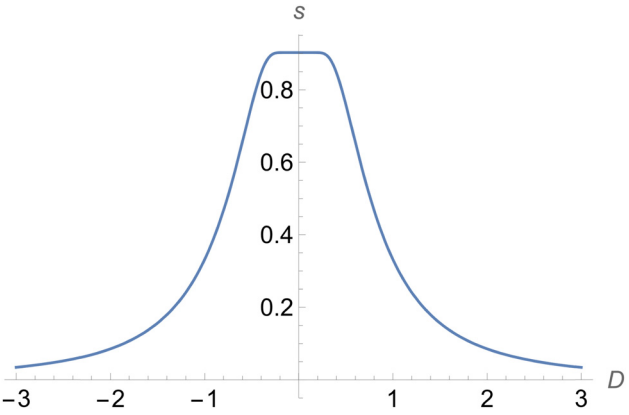

Figure 5: The scaled Stark profile $s(D)$ of the Ly-alpha π-component (given by Eq. (35)) *vs* the scaled detuning D (given by Eq. (36)) for the situation where the scaled electric field F (represented by the quasistatic part of the ion microfield) is much smaller than the magnetic field M (both fields are defined in Eq. (17)) [10].

We note in passing that after paper [10] was published in January 2023, paper [47] was published by another author in September 2023. In that paper there was an unintentional overlap with some equations from paper [10] without the reference to paper [10].

4 Intra-Stark spectroscopy

In Section 1, we described the ISS only very briefly. Here we start by presenting more details.

The Langmuir-wave-caused "dip" in spectral line profiles, where the word "dip," used for brevity, refers to a highly-localized *structure* in the line profile – the structure consisting of a local minimum of the intensity surrounded by two "bumps" (peaks) – is an *emergent phenomenon* that springs from *multifrequency nonlinear dynamic resonances* (*e.g.*, [13,15] and books [2,7]). The analytical predictions of the emergent phenomenon of the Langmuir-wave-caused "dips" were confirmed in a large number of experiments by various experimental groups working at different plasma machines, as well as in astrophysical observations. In these experiments and observations, that span the range of the electron densities about ten orders of magnitude, the Langmuir-wave-caused highly-localized structures were reliably detected, identified, and used for plasma diagnostics. This included, in particular, the high-precision, benchmark experiments at the gas-liner pinch [14,48], where plasma

parameters were measured by the coherent Thomson scattering independent of the measurements of the line profiles.

Nevertheless, a recent study by Alexiou [49] indicated that there is still the confusion on the ISS. Therefore, here we clarify the confusion for the entire research community and provide new analytical results on this subject.

The physics behind the Langmuir-wave-caused structures is as follows. Let us consider the electric field

$$\mathbf{E}(t) = \mathbf{F} + \mathbf{E}_0 \cos(\omega t), \tag{39}$$

where $\mathbf{F}$ represents the quasistatic part of the electric field in the plasma. The field $\mathbf{F}$ could have not only the contribution from the quasistatic part of the ion microfield, but also the contribution from the LEPT (such as the ion acoustic waves, lower hybrid waves, or Bernstein modes). If $\mathbf{F}$ and $\mathbf{E}_0$ are not collinear (which is true for the overwhelming majority of possible mutual orientations of vectors $\mathbf{F}$ and $\mathbf{E}_0$), then the total field $\mathbf{E}(t)$ is *librating*. The frequency spectrum of this librating field consists not only of the frequency ω, but also of its *harmonics*: the frequency spectrum of the librating field is $u\omega$, where $u = 1, 2, 3, ...$

We denote the absolute value of the total electric field averaged over the period of the libration by $F_{\rm eff}$.

$$F_{\rm eff} = \langle |\mathbf{E}(t)| \rangle. \tag{40}$$

If the librating nature of the total electric field would be first disregarded, the energy levels of a radiating hydrogenic atom/ion (the radiator) of the nuclear charge Z_r would split into $2n - 1$ Stark sublevels separated by (in the atomic units)

$$\Omega = 3nF_{\rm eff}/(2Z_r), \tag{41}$$

where n is the principal quantum number. The Stark sublevels are distinguished by the electric quantum number

$$q = n_1 - n_2, \tag{42}$$

where n_1 and n_2 are the parabolic quantum numbers.

The combined system "radiator + field" can be described in terms of quasienergy states (introduced by Zeldovich [50] and Ritus [51]), whose quasienergies Q are as follows:

$$Q = \Omega + v\omega, \quad v = 0, \pm 1, \pm 2, \pm 3, ... \tag{43}$$

Now we take into account the time-dependent component of the librating electric field. We remind that its frequency spectrum is $u\omega$, where $u = 1, 2, 3, ...$ Here we come to the central point. In the situation, where

$$\Omega = u\omega, \quad u = 1, 2, 3,..., \tag{44}$$

there occur multiple *resonances between the harmonics of the librating field and all quasienergy states of the quasienergies* $Q = \Omega + v\omega$. In other words, the resonances are *multiquantum* (in terms of the quanta of the Langmuir field) and *multifrequency*. It causes the degeneracy of all quasienergy states: the quasienergy harmonics, resulting from each of the $2n - 1$ atomic Stark substates, superimpose with each other.

In this multiquantum multifrequency resonance, each degenerate quasienergy state is a superposition of several quasienergy harmonics originating from different Stark sublevels (sublevels of different values of the electric quantum number q). The Stark sublevel of some value of q is coupled by the dipole matrix element with the sublevels of $q + 1$ and $q - 1$. As a result of this coupling, there occurs an additional splitting of *all* quasienergy harmonics. This splitting has an analogy with the Rabi splitting, but it is its generalization for the case of the multiquantum multifrequency resonances. The additional splitting of *all* quasienergy harmonics is generally a *nonlinear* function of the Langmuir field amplitude E_0 (e.g., Eq. (9) from the study by Gavrilenko and Oks [13]).

The multiquantum multifrequency resonances corresponds to a set of specific locations in the profile of a hydrogen-like spectral line – because they correspond to specific resonance values of $F_{\rm eff}$ satisfying the condition (44). These locations are separated from the center of the spectral line by the well-defined amounts of the wavelength $\Delta\lambda^{\rm dip}(\omega)$, where $\Delta\lambda^{\rm dip}(\omega)$ are well-defined functions of the Langmuir wave frequency $\omega = (4\pi e^2 N_e/m_e)^{1/2}$, so that (*e.g.*, [2,7])

$$\Delta\lambda^{\rm dip} = aN_e^{1/2} + bN_e^{3/4}, \tag{45}$$

where the coefficients a and b are controlled by the quantum numbers and by the charges of the radiating and perturbing ions. The identification of these structures in the experimental line profile allows a very accurate determination of the electron density N_e from the locations of these structures.

At each exact location in the line profile, corresponding to the resonance (44), (for brevity, the "resonance location") due to the generalized Rabi splitting of the quasienergies, there occurs a partial transfer of the intensity from the wavelength of the exact resonance location to adjacent wavelengths on each side of the exact resonance location. As a result, there can appear a structure consisting of the local depression of the intensity surrounded by two relatively small "bumps," as illustrated in Figure 6.

Being superimposed with an inclined "unperturbed" spectral profile, *each bump-dip-bump structure can be responsible for two local minima of the intensity* – as shown in Figure 6 – rather than just for one local minimum of the intensity.

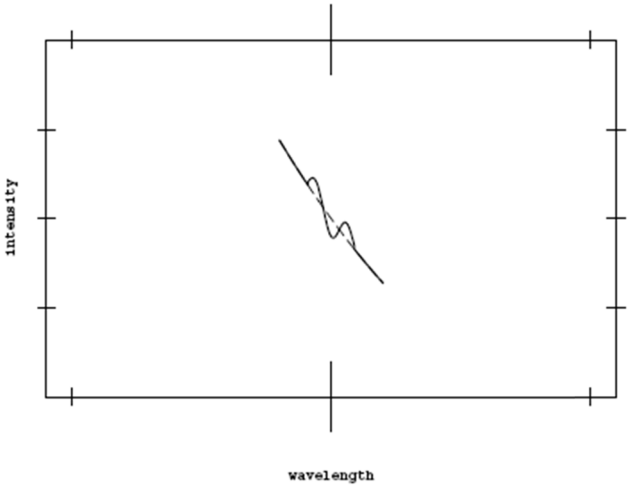

Figure 6: Sketch of the calculated "bump-dip-bump" structure, caused by the multifrequency nonlinear dynamic resonance (44), superimposed with an inclined "unperturbed" spectral line profile.

The secondary minimum located at the higher intensity than the primary minimum is of no physical significance. Sometimes one of the two bumps and/or the secondary local minimum manifests only as a small "shoulder."

The analytically predicted Langmuir-wave-caused "dips" were then revealed in a large number of various experiments around the world [14,16,18,48,52–59] and in astrophysical observations [60]. In these experiments and observations, the Langmuir-wave-caused "dips" were reliably detected, identified, and used for plasma diagnostics in plasmas of the electron density ranging from $10^{13}\,\mathrm{cm}^{-3}$ to $3 \times 10^{22}\,\mathrm{cm}^{-3}$.

For example, in the high-precision, benchmark experiments by the Kunze group at the gas-liner pinch [14,48], where plasma parameters were measured by the coherent Thomson scattering independent of the measurements of the line profiles, first, the existence of the Langmuir-wave-caused "dips" was reliably established, the evolution of their positions as the electron density varied being consistent with the theory. Second, detailed bump-dip-bump structure in the line profile was revealed experimentally for the first time – Figure 7.

Third, it was also demonstrated that the experimental dip positions yielded the values of the electron density just as accurate as the electron density measured by the coherent Thomson scattering – Figure 8.

Thus, all theoretical predictions from previous studies [13,15] (as well as from subsequent works covered in books [2,7]), concerning the multifrequency nonlinear dynamic resonances and the resulting bump-dip-bump structures in spectral line profiles, have been confirmed and used for plasma diagnostics at numerous experiments around the world.

Now we review some details from previous studies [19–21] that presented new analytical results on the ISS. In these works, there were offered three new, L-dip-based spectroscopic methods for measuring the GigaGauss magnetic fields developing during the relativistic laser–plasma interaction.

L-dips are the consequence of the dynamic resonance between the Stark splitting

$$\omega_{\mathrm{stark}}(F) = 3n\hbar F/(2Z_{\mathrm{r}}m_{\mathrm{e}}e), \tag{46}$$

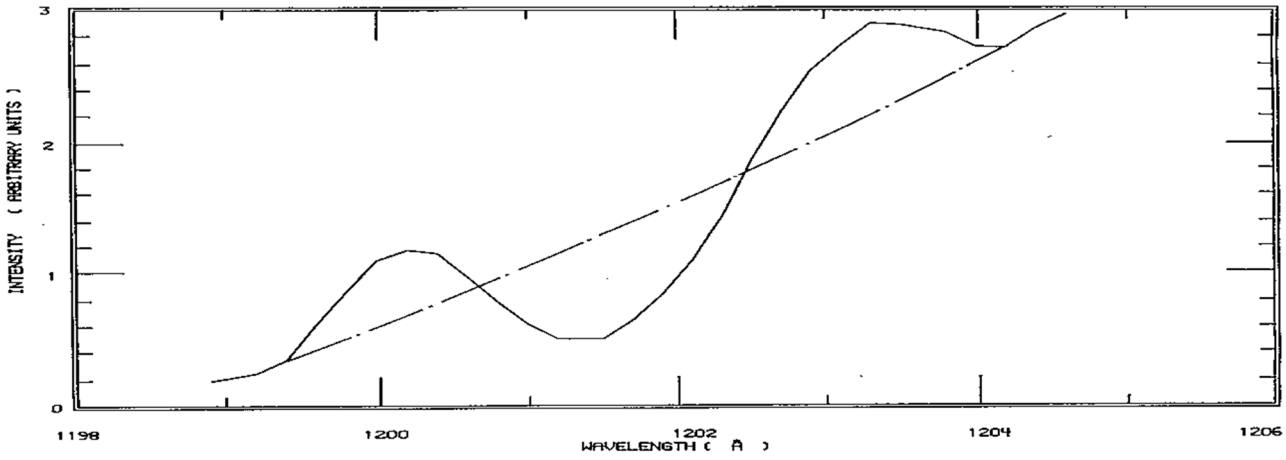

Figure 7: A magnified part of the profile of the Ly-alpha line, obtained in the high-precision, benchmark experiment at the gas-liner pinch [14], showing the observed bump-dip-bump structure. The electron density was $2.1 \times 10^{18}\,\mathrm{cm}^{-3}$ and the electron temperature was about 10 eV.

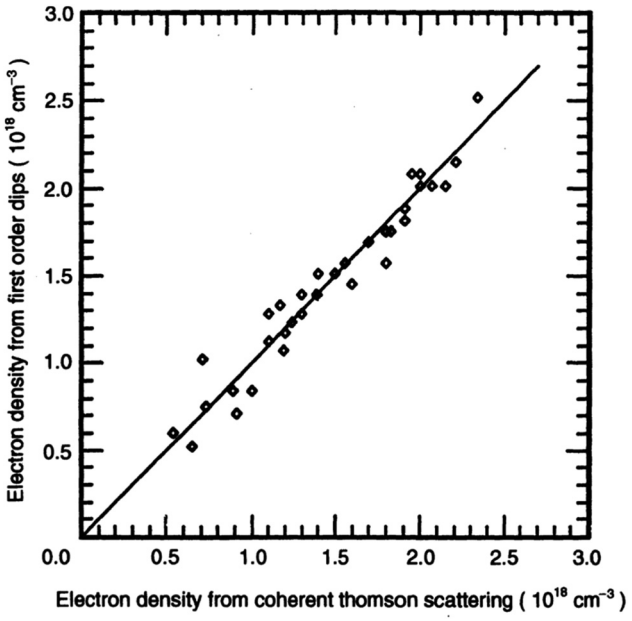

Figure 8: Electron densities obtained from the experimental positions of the Langmuir-wave-caused bump-dip-bump structures *vs* the electron densities measured by the coherent Thomson scattering. The comparison is shown at many electron densities in the experiments at the gas-liner pinch [14]. The range of the electron densities was (0.5–2.5) × 10^{18} cm^{-3} and the electron temperature was about 10 eV.

of hydrogenic energy levels (F being the quasistatic part of the electric field in a plasma) and the frequency ω_L of the Langmuir wave, the latter frequency practically coinciding with the plasma electron frequency $\omega_{pe} = (4\pi e^2 N_e/m_e)^{1/2}$:

$$\omega_{stark}(F) = s\omega_{pe}(N_e), \quad s = 1, 2, \ldots, \tag{47}$$

where s is the number of the Langmuir quanta involved in the resonance, while Z_r and n are the nuclear charge and the principal quantum number of the radiating hydrogenic atom or ion (radiator). While the applied electric field is quasimonochromatic, there arises a nonlinear dynamic resonance of a multifrequency nature, as elucidated in the study by Gavrilenko and Oks [15].

In the previous studies [19–21], the authors considered the situation where there is also a magnetic field **B** in plasmas. By generalizing the results from the study by Gavrilenko [61], Dalimier and Oks [19] obtained the following formulas for the location of the two sets of the L-dips in the spectral line profiles:

$$\Delta\omega_{dip}^{(\alpha)} = s\omega\{(n' + n'')_\alpha - [(n' + n'')_\beta /n_\alpha][(n_\alpha^2 - n_\beta^2)b^2 + n_\beta^2]^{1/2}\}, \tag{48}$$

$$\Delta\omega_{dip}^{(\beta)} = s\omega\{[(n' + n'')_\alpha/n_\beta][n_\alpha^2 - (n_\alpha^2 - n_\beta^2)b^2]^{1/2} - (n' + n'')_\beta\}, \tag{49}$$

where the quantum numbers n' and n'' correspond to the basis of the wave functions diagonalizing the Hamiltonian of a hydrogen atom in a non-collinear static electric and magnetic fields [33]):

$$n', n'' = -j, -j + 1, \ldots, j; \quad j = (n - 1)/2, \tag{50}$$

where subscripts α and β label the upper and lower substates engaged in the radiative transition.

The locations of the two sets of the L-dips from Eqs (48) and (49) depend on the following scaled dimensionless magnetic field:

$$b = \mu_0 B/(s\hbar\omega) = (1/s)[B(GG) /0.201][\omega(s^{-1})/(1.77 \times 10^{15})]^{-1}. \tag{51}$$

For instance, for the one-quantum resonance (s = 1), for the frequency $\omega = 1.77 \times 10^{15}$ s^{-1} being used, *e.g.*, in experiments [52,58], the quantity b reaches unity at B = 0.201 GG.

Thus, the magnetic field **B** shifts the positions of the L-dips compared to B = 0. The idea of a new method by Dalimier and Oks [19] for measuring the magnetic fields was described in their work as follows:

"It is possible to select such a pair of the L-dip at $\Delta\omega_{dip}^{(\alpha)}$ and the L-dip at $\Delta\omega_{dip}^{(\beta)}$, both corresponding to the same combination of the sums $(n' + n'')_\alpha$ and $(n' + n'')_\beta$, such that the location of one of the two L-dips is unaffected by the magnetic field while the location of the other of the two L-dips is shifted by the magnetic field. Then from the relative separation of the two L-dips it is possible to determine the magnetic field."

Specifically, the focus was on the following pairs of the L-dips. One pair corresponding to

$$(n' + n'')_\alpha = 0, (n' + n'')_\beta = -1, \tag{52}$$

and another pair corresponding to

$$(n' + n'')_\alpha = 1, (n' + n'')_\beta = 0. \tag{53}$$

The ratio

$$\Delta\omega_{dip}^{(\alpha)}/\Delta\omega_{dip}^{(\beta)} = (1/n_\alpha)[(n_\alpha^2 - n_\beta^2)b^2 + n_\beta^2]^{1/2} \tag{54}$$

for the first pair and the ratio

$$\Delta\omega_{dip}^{(\beta)}/\Delta\omega_{dip}^{(\alpha)} = (1/n_\beta)[n_\alpha^2 - (n_\alpha^2 - n_\beta^2)b^2]^{1/2}, \tag{55}$$

for the second pair are simple functions of the magnetic field, as one can see from Eqs (54) and (55).

Figure 9 displays the ratio $\Delta\omega_{dip}^{(\alpha)}/\Delta\omega_{dip}^{(\beta)}$ in the pair of the L-dips corresponding to $(n' + n'')_\alpha = 0, (n' + n'')_\beta = -1$ *vs* the scaled dimensionless magnetic field b for the Balmer-alpha line (solid curve) and for the Balmer-beta line (dashed curve).

From Figure 9, one can see that in the range of b, the magnetic field strongly changes the relative positions of the L-dips, so that by measuring the latter, it is feasible to determine the magnetic field. For the laser frequency $\omega = 1.77 \times 10^{15}$ s^{-1}, the range of $b \sim$ (1–10) translates to the range of the magnetic field $B \sim$ (0.2–2) GG for the case of the one-quantum resonance and to $B \sim$ (0.4–4) GG for the case of the two-quantum resonance.

Oks *et al.* [20] focused on another way for the Giga-Gauss magnetic fields to affect the L-dips: their effect on the halfwidth of the L-dips. The scaled dimensionless halfwidth $w_s = \delta\omega_{dip}^{(s)}/\omega$ of the L-dips can be represented in the form

$$w_s = \delta\omega_{dip}^{(s)}/\omega = [e/(Z_r\hbar\omega)]|z_{12}|sE_0J_s(u)/u, \quad u = [e/(Z_r\hbar)](z_{11} - z_{22})E_0/\omega, \tag{56}$$

where $J_s(u)$ is the Bessel function. The matrix elements z_{12}, z_{11}, z_{22} were calculated for the Ly-alpha line on the basis of the wave functions from the study by Demkov *et al.* [33]. These wave functions are linear combinations of the corresponding parabolic wave functions. The coefficients of the linear combinations are products of the Wigner d-functions: namely, the functions $d_{p,\ \pm 1/2}{}^{1/2}(\alpha_1)$ and $d_{p,\ \pm 1/2}{}^{1/2}(\alpha_2)$, where $p = n', n''$. The angles α_1 and α_2 can be expressed in the following form:

$$\alpha_1 = \tan^{-1}\{\sin\alpha/[\cos\alpha - Z_r m_e e\mu_0 B/(3\hbar^2 F)]\}, \quad \alpha_2 = \tan^{-1}\{\sin\alpha/[\cos\alpha + Z_r m_e e\mu_0 B/(3\hbar^2 F)]\}, \tag{57}$$

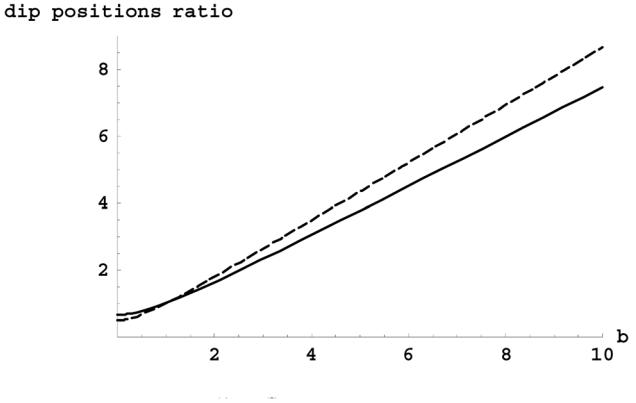

Figure 9: The ratio of positions $\Delta\omega_{dip}^{(\alpha)}/\Delta\omega_{dip}^{(\beta)}$ in the pair of the L-dips corresponding to $(n' + n'')_\alpha = 0$, $(n' + n'')_\beta = 1$ *vs* the scaled (dimensionless) magnetic field b (defined by Eq. (51)) for the Balmer-alpha line (solid curve) and for the Balmer-beta line (dashed curve) [19]. For instance, for the one-quantum resonance, for the frequency $\omega = 1.77 \times 10^{15}$ s^{-1} being used, *e.g.*, in experiments [52,58], the quantity b reaches unity at $B = 0.201$ GG. Copyright Dalimier and Oks 2018.

where α is the angle between vectors **B** and **F**. Thus, the angles α_1 and α_2 explicitly depend on the magnetic field.

In the study by Oks *et al.* [20], the following three dimensionless quantities were also defined:

$$b_0 = \mu_0 B/(\hbar\omega), \quad \gamma = \hbar E_0/(Z_r m_e e\omega), \quad f = \hbar F/(Z_r m_e e\omega), \tag{58}$$

where b_0 is the scaled magnetic field, γ is the scaled amplitude of the Langmuir wave, and f is the scaled quasistatic electric field. Then, it was possible to rewrite the scaled halfwidth w_s from Eq. (56) as follows:

$$w_s = (|z_{12}|/a_0)s\gamma J_s(u)/u, \quad u = \gamma(z_{11} - z_{22})/a_0, \tag{59}$$

where a_0 is the Bohr radius. The formulas for angles α_1 and α_2 from Eq. (57) was also simplified:

$$\alpha_1 = \tan^{-1}\{\sin\alpha/[\cos\alpha - b_0/(3f)]\}, \quad \alpha_2 = \tan^{-1}\{\sin\alpha/[\cos\alpha + b_0/(3f)]\}. \tag{60}$$

Thus, the halfwidth of the L-dips, which at the absence of the magnetic field was controlled only by the amplitude E_0 of the Langmuir wave, becomes controlled by B, E_0, and F in strongly magnetized plasmas (here F is the quasistatic part of the plasma electric field). The results from the study by *Oks et al.* [20] formed the basis for another new method for measuring super-strong magnetic fields.

The employment of the effect of the super-strong magnetic fields on the width of the L-dips makes it possible to measure such fields by using x-ray Lyman lines – the lines usually studied in laser–plasma interaction experiments. This was advantageous in comparison to the method by Dalimier and Oks [19] that was applicable only to non-Lyman lines (such as the Balmer lines).

Dalimier *et al.* [21] put forward yet another new L-dip-based method for measuring the super-strong magnetic fields developing in the relativistic laser–plasma interactions. This method relates to the situation where the mid-point between the pair (or pairs) of the experimental L-dip-structures in the line profile is shifted.

In the absence of the LEPT, for the electron densities $N_e > 10^{22}$ cm^{-3}, the mid-point between the two L-dips in the pair would be red-shifted due to the spatial non-uniformity of the ion microfield at the location of the radiating ions [7,14]. This shift increases with N_e and for sub-solid-state densities could reach several tens of mÅ. This situation, as well as the intermediate scenario (where the ion microfield and the LEPT have comparable strengths) could occur at laser intensities higher than 2×10^{20} W/cm^2.

Here is the step-by-step algorithm for using this new method.

1. From the experimental separation between a pair of the L-dip structures, to determine the electron density N_e

with high accuracy. This enables also to calculate the characteristic strength of the ion microfield F_{ion}.

2. From the shift of the mid-point between the pair (or pairs) of the L-dip-structures, knowing the characteristic strength of the ion microfield (from step 1), to determine the characteristic strength F_{LEPT} of the LEPT (if any).
3. Knowing the F_{ion} and F_{LEPT} from steps 1 and 2, to calculate the FWHM of the theoretical Stark profile, including also the broadening by plasma electrons: $\Delta\lambda_{1/2S}$. The temperature required for calculating the contribution by plasma electrons can be estimated as T(eV) ~ $2.5Z^2$, where Z is the nuclear charge of the radiating ions. This estimate of T typically has the accuracy of about 20%. For the broadening by plasma electrons, which scales as ~ $1/T^{1/2}$, formula T(eV) ~ $2.5Z^2$ would therefore yield the accuracy of about 10%. This accuracy is sufficient especially because for the plasmas created by relativistic laser–plasma interactions, the broadening by plasma electrons is small compared to the broadening by the LEPT and/or the ion microfield.
4. For plasmas created during relativistic laser–plasma interactions, the Stark broadening of the hydrogenic X-ray spectral lines usually predominates over the Doppler broadening. However, the Doppler broadening can be added for calculating the FWHM of the Stark-Doppler theoretical profile $\Delta\lambda_{1/2SD}$ by using the estimate T(eV) ~ $2.5Z^2$. Since Doppler broadening scales as ~ $T^{1/2}$, formula T(eV) ~ $2.5Z^2$ would therefore yield the accuracy of about 10%. This accuracy is sufficient especially because for the plasmas created by relativistic laser–plasma interactions, the Doppler broadening is small compared to the broadening by the LEPT and/or the ion microfield.
5. If the FWHM of the theoretical profile $\Delta\lambda_{1/2SD}$ is noticeably smaller than the FWHM of the experimental profile $\Delta\lambda_{1/2exp}$, the next step would be to check whether the experimental profile is affected by some opacity. For the example of the Ly-beta line, if the top of the experimental profile exhibits the doublet structure (typical for the theoretical profiles of the Ly-beta line), then the optical depth at the top of the profile is $\tau_0 << 1$, so that the opacity cannot make a noticeable contribution to the FWHM of the experimental profile.
6. If in step 5 it would be established that $\tau_0 << 1$, then this would prove that the noticeable excess of the experimental FWHM $\Delta\lambda_{1/2exp}$ compared to the FWHM $\Delta\lambda_{1/2SD}$ of the theoretical Stark-Doppler profile is due to a magnetic field. The strength B of the magnetic field can be deduced from the difference ($\Delta\lambda_{1/2exp} - \Delta\lambda_{1/2SD}$) by using the standard formula for the Zeeman effect for hydrogenic spectral lines.

It is important to emphasize that the above algorithm allows determining the presence of the magnetic field and its strength B without the detailed modeling of the entire experimental profile. The subsequent modeling would only make the determination of the magnetic field strength B slightly more accurate.

Dalimier *et al.* [21] also emphatically underscored that in many cases, modulations in some experimental profile of a hydrogenic line have nothing to do with the L-dip phenomenon. The process of establishing whether the modulations in some experimental profile of a hydrogenic spectral line are related to L-dip structures involves multiple tests of self-consistency, as follows.

Test #1. L-dip structures (if any) should appear both in the red and blue parts of the experimental profile and (in the first approximation) should be approximately symmetric with respect to the line center.

Test #2. The value of N_e, determined from the separation between these two structures (one in the red part, another in the blue part) should make sense physically at least by the order of magnitude. (This separation is controlled by the Langmuir wave frequency, which in its turn is controlled by N_e.)

Test #3. If there is more than one pair of such structures, then the values of N_e, determined from the separation within the two different pairs, should coincide.

Test #4. If there is a red shift of the mid-point within the pair of structures, then the values of N_e, determined from the mid-point-shift for two different structures, should coincide.

Test #5. The separation within the pair of such structures also determines the resonant value F_{res} of the quasi-static electric field (involved together with the Langmuir field in the production of the L-dip structure). The half-width of the L-dip-structure determines the amplitude E_0 of the Langmuir field. Then, the condition $E_0 < F/2$ should be met. Otherwise, according to the theory by Oks [7], no L-dip structures can be produced.

Test #6. All local minima and maxima in the experimental profile should be explained by L-dip structures – except for far wings dominated by the noise (once again, one L-dip structure can explain up to two local minima and two local maxima of intensity.)

Only after all the above six tests would be successfully passed, one can proceed with applying the new L-dip-based methods for measuring GigaGauss magnetic fields.

Finally, we provide some details on the confusion by Alexiou [49] concerning the physics behind the ISS. In the study by Alexiou [49], there were presented simulations ignoring the actual nature of the Langmuir-wave-caused dips. This led to the inability to reproduce them for the experimental spectral line profiles from the study by Oks

et al. [52]: the work describing the project on spectroscopic diagnostics of the relativistic laser–plasma interactions – the project resulting from the collaboration of experimentalists and theorists from seven countries (Japan, the UK, France, Germany, Hungary, the USA, and Russia). Since Alexiou [49] showed the confusion on this subject, for the benefit of other researchers we highlight below the various points of the confusion.

A. The primary flaw of simulations from the study by Alexiou [49] is the following: there was no understanding of the nature of the *emergent phenomenon* of Langmuir-wave-caused "dips" as stemming from the *multifrequency nonlinear dynamic resonance*. This kind of the resonance effects was beyond the code used by Alexiou [49]. From the outset, that code was tied to Blochinzew satellites (theoretically predicted by Blochinzew in 1933 [62]). What was called "dips" in the study by Alexiou [49] are in fact just random *troughs between the peaks*, where the peaks are (shifted) Blochinzew satellites. The definition of the "dips" by Alexiou [49] has nothing to do with the highly-localized structures in spectral line profiles caused by the multifrequency nonlinear dynamic resonances.

For a given hydrogenic spectral line, a given nuclear charge of the radiator, and a given charge of the perturbing ions, the locations of these structures (the Langmuir wave-caused "dips") are controlled by the electron density N_e (which is why from the experimental locations of these structures one can deduce N_e with the same accuracy as if N_e would be measured by the Thomson scattering). In distinction, the locations of the random troughs in the study by Alexiou [49] between the Blochinzew peaks (the troughs confused with the above structures manifesting the multifrequency nonlinear dynamic resonances) result from the interplay of many plasma parameters and practically cannot be used for determining the electron density. Just this primary flaw of the simulations [49] would be the sufficient cause of the inability to fit the experimental data in the study by Oks *et al.* [52] (that were attempted to fit in the study by Alexiou [49]).

By the way, it should be also clarified that under the condition $E_0 << F_{eff}$ (where F_{eff} is the absolute value of the total electric field $\mathbf{E}(t) = \mathbf{F} + \mathbf{E}_0 \cos(\omega t)$, averaged over the period of the libration) typical for all experiments in plasmas containing Langmuir waves, the observed local structures in the profiles can be only the Langmuir-wave-caused "dips," rather than Blochinzew satellites, as explained in detail in Section 7.1 of book [7]. Blochinzew satellites could be observed in the "underdense" regions of laser-produced plasmas where these satellites would be caused by the laser field, rather than by the field of the Langmuir waves. These are the regions below the critical electron density where the laser radiation can propagate inside the plasma and cause the situation where the laser amplitude significantly exceeds the quasistatic electric field in the plasma.

In general, computational simulations (codes), being only a model of nature, not nature itself, usually fail to capture emergent phenomena (and lack the physical insight) – *e.g.*, [8]. The primary advantage of analytical calculations over codes is that the former can capture emergent phenomena while the latter usually cannot.

B. In the study by Alexiou [49], the experimental spectra presented in parts A, B, and C of Figure 3 from the study by Oks et al. [52] were qualified as "noisy." This indicates again the lack of the understanding that the Langmuir-wave-caused "dip" is the structure consisting of the local minimum of the intensity (at the location controlled by the electron density) surrounded by two local maxima ("bumps") plus the secondary minimum. With the understanding of this structure of each "dip," all local minima and maxima of the intensity in parts A, B, and C of Figure 3 from the study by Oks *et al.* [52] have been identified, accounted for, and clearly indicated. Besides, the bump-to-dip ratio of the intensities was up to 45%, thus exceeding the noise level by at least one order of magnitude. No wonder that the experimental spectra, obtained with a high spectral resolution ($\lambda/\delta\lambda \sim 3{,}000$), easily allowed the reliable and the only one possible identification of the above structures.

C. Another flaw of simulation in the study by Alexiou [49] is the following. There was also the lack of understanding that regardless of the specific distribution of the quasistatic field $\mathbf{F}$ over its magnitude and its direction, there is always a small group of radiators in the ensemble, for which the Stark splitting by the field $\mathbf{F}$ is in the multiquantum/multifrequency resonance with the frequency of the Langmuir field $\mathbf{E}_0 \cos(\omega t)$ and its harmonics. Therefore, the locations of the resulting highly localized structures in the spectral line profiles do not depend on the specific distribution of the quasistatic field $\mathbf{F}$ – in distinction to the locations of the random troughs between (shifted) Blochinzew satellites, calculated in the study by Alexiou [49].

D. In the study by Alexiou [49], there was also a claim that distribution functions of the turbulent fields are not known. However, in reality, the distribution functions of the quasistatic turbulent fields had been derived analytically by Oks and Sholin [43] already in 1976.

E. Besides, in the study by Alexiou [49], it was claimed that that work was the first to reveal that in plasmas containing Langmuir waves, the spectral line profiles exhibit directional/polarization effects. However, already in 1977, Oks and Sholin [63] showed analytically that the highly localized structures in spectral line profiles, emitted from such plasmas due to the above dynamical resonances,

exhibit directional/polarization effects. Moreover, in the same year 1977, these polarization effects have been confirmed experimentally and used for plasma diagnostics by Zhuzhunashvili and Oks [53].

5 Conclusion

We reviewed the recent analytical advances in the spectroscopy of hydrogenic spectral lines in plasmas. The review covered the following topics where the recent advances were made.

First, we reviewed the analytical solution by Oks *et al.* [9] for the splitting of hydrogenic spectral lines under the combination of a circularly polarized electromagnetic wave with a strong magnetic field. One of the counterintuitive results obtained by Oks *et al.* [9] was the possibility of decreasing the splitting of hydrogenic spectral lines by changing the magnetic field. This was a *counterintuitive* result. Another counterintuitive result was that by the proper choice of the magnetic field, the total intensity of the spectral line can diminish by 40%. Practical applications of these results relate to the spectroscopic diagnostic of the electron cyclotron waves (used as an additional heating method for plasmas in magnetic fusion machines) and to the relativistic laser plasma interactions.

Second, we reviewed the analytical results from the study by Oks [10] concerning the Stark–Zeeman broadening of the Ly-alpha line in plasmas. The focus was on the remarkable properties of the π-component of the Ly-alpha line. In the study by Oks [10], it was found that in the situation where the Zeeman effect dominates over the Stark effects the broadening of the Ly-alpha π-component is controlled by the linear Stark effect – while this was not the case for the Ly-alpha σ-component or any component of any other hydrogenic spectral line. These results open the way for the Stark width of the Ly-alpha π-component to be used in this situation for the experimental determination of the ion density or of the root-mean-square field of a LEPT.

Third, we reviewed recent analytical advances in the area of the ISS. In the previous studies [19–21], three new different methods were presented, based on the emergent phenomenon of the Langmuir-wave-caused structures ("L-dips") in the line profiles, for measuring super-strong magnetic fields of the GigaGauss or even multi-GigaGauss range developed at the surface of the relativistic critical density during relativistic laser–plasma interactions. We also reviewed the rich physics behind the L-dips phenomenon – because there was the confusion in the literature in this regard.

For further reading on the related subjects, we refer to previous studies [35,64–120].

Funding information: The authors state no funding involved.

Author contributions: All authors have accepted responsibility for the entire content of this manuscript and approved its submission.

Conflict of interest: The authors state no conflict of interest.

References

[1] Oks E. Advances in x-ray spectroscopy of laser plasmas. Bristol, UK: IOP Publishing; 2020.
[2] Oks E. Diagnostics of laboratory and astrophysical plasmas using spectral lineshapes of one-, two-, and three-electron systems. Singapore: World Scientific; 2017.
[3] Kunze HJ. Introduction to plasma spectroscopy. Berlin: Springer; 2009.
[4] Oks E. Stark broadening of hydrogen and hydrogenlike spectral lines in plasmas: the physical insight. Oxford, UK: Alpha Science International; 2006.
[5] Fujimoto T. Plasma spectroscopy. Oxford, UK: Clarendon Press; 2004.
[6] Griem HR. Principles of plasma spectroscopy. Cambridge: Cambridge University Press; 1997.
[7] Oks E. Plasma spectroscopy: the influence of microwave and laser fields. New York: Springer; 1995.
[8] Post DE, Votta LG. Computational science demands a new paradigm. Phys Today. 2005;58(1):35–41.
[9] Oks E, Angelo P, Dalimier E. Magnetic-field-caused narrowing of hydrogenic spectral lines under a circularly polarized electromagnetic wave: the analytical solution. Eur Phys J Plus. 2023;138:884.
[10] Oks E. Analytical results for the Stark-Zeeman broadening of the Lyman-alpha line in plasmas. Int Rev Atomic Mol Phys. 2023;14:43–8.
[11] Derevianko A, Oks E. A generalized theory of ion impact broadening in magnetized plasmas and its applications for tokamaks. Phys Rev Lett. 1994;73:2059–62.
[12] Derevianko A, Oks E. Dual-purpose diagnostics of the edge plasmas of tokamaks based on a novel spectroscopic effect. Rev Sci Instrum. 1997;68:998–1001.
[13] Gavrilenko VP, Oks E. Intra-Stark spectroscopy of Coulomb emitters in plasmas containing quasimonochromatic electric fields. Sov Phys J Plasma Phys. 1987;13:22–8.
[14] Oks E, Böddeker St, Kunze HJ. Spectroscopy of atomic hydrogen in dense plasmas in the presence of dynamic fields: intra-Stark spectroscopy. Phys Rev A. 1991;44:8338–47.
[15] Gavrilenko VP, Oks E. A new effect in the Stark spectroscopy of atomic hydrogen: dynamic resonance. Sov Phys JETP. 1981;53:1122–7.
[16] Dalimier E, Oks E, Renner O. Review of Langmuir-wave-caused dips and charge-exchange-caused dips in spectral lines from plasmas and their applications. Atoms. 2014;2:178.
[17] Dalimier E, Faenov A, Oks Y, Angelo E, Pikuz P, Fukuda TA, et al. X-ray spectroscopy of super-intense laser-produced plasmas for the study of nonlinear processes. Comparison with PIC simulations. J Phys Conf Ser. 2017;810:012004.

[18] Dalimier E, Oks E, Renner O. Dips in spectral line profiles and their applications in plasma physics and atomic physics. AIP Conf Proc. 2017:1811:190003
[19] Dalimier E, Oks E. X-ray spectroscopy-based diagnostic of GigaGauss magnetic fields during relativistic laser-plasma interactions. Atoms. 2018;6:60.
[20] Oks E, Dalimier E, Angelo P. Effects of ultraintense magnetic fields due to relativistic laser-plasma interactions on Langmuir-wave-caused dips in x-ray spectral line profiles. Spectrochim Acta, Part B. 2019;157:1–5.
[21] Dalimier E, Oks E, Angelo P. Alternative principle for measuring GigaGauss magnetic fields during relativistic laser-plasma interactions by analyzing x-ray spectral lineshapes. Int Rev Atomic Mol Phys. 2020;11:1–6.
[22] Belyaev VS, Krainov VP, Lisitsa VS, Matafonov AP. Generation of fast charged particles and superstrong magnetic fields in the interaction of ultrashort high-intensity laser pulses with solid targets. Physics – Uspekhi. 2008;51:793–814.
[23] Belyaev VS, Matafonov AP. Fast charged particles and superstrong magnetic fields generated by intense laser target interaction. In: Andreev A, editor. Femtosecond-scale optics. Shanghai: InTech; 2011. p. 87–112.
[24] Wagner U, Tatarakis M, Gopal A, Beg FN, Clark EL, Dangor AE, et al. Laboratory measurements of 0.7 GG magnetic fields generated during high-intensity laser interactions with dense plasmas. Phys Rev E. 2004;70:e026401.
[25] Tatarakis M, Gopal A, Watts I, Beg FN, Dangor AE, Krushelnik K, et al. Measurements of ultrastrong magnetic fields during relativistic laser–plasma interactions. Phys Plasmas. 2022;9:2244–50.
[26] Tatarakis M, Watts I, Beg FN, Clark EL, Dangor AE, Gopal A, et al. Measuring huge magnetic fields. Nature. 2002;415:280.
[27] Kato S, Nakamura T, Mima K, Sentoku Y, Nagatomo H, Owadano Y. Generation of quasistatic magnetic field in the relativistic laser-plasma interactions. J Plasma Fusion Res. 2004;6:658–61.
[28] Perogaro F, Bulanov SV, Califano F, Esirkepov TZh, Lontano M, Meyer-ter-Vehn J, et al. Magnetic fields from high-intensity laser pulses in plasmas. Plasma Phys Control Fusion. 1997;38:B261–72.
[29] Singh M, Gopal K, Gupta D. Temporally asymmetric laser pulse for magnetic-field generation in plasmas. Phys Lett A. 2016;380:1437–41.
[30] Liseykina TV, Popruzhenko SV, Macchi A. Inverse Faraday effect driven by radiation friction. New J Phys. 2016;18:e072001.
[31] Santos JJ, Bailly-Crandvaux M, Ehret M, Arefiev AV, Batani D, Beg FN, et al. Laser-driven strong magnetostatic fields with applications to charged beam transport and magnetized high energy-density physics. Phys Plasmas. 2018;25:e056705.
[32] Lisitsa VS. Hydrogen atom in the rotating electric field. Opt Spectrosc. 1971;31:468–71.
[33] Demkov Y, Monozon BS, Ostrovsky VN. Energy levels of a hydrogen atom in crossed electric and magnetic fields. Sov Phys JETP. 1970;30:775–6.
[34] Fock V. Zur theorie des wasserstoffatoms. Z Physik. 1935;98:145.
[35] Lisitsa VS, Sholin GV. Exact solution of the problem of the broadening of the hydrogen spectral lines in the one-electron theory. Sov Phys JETP. 1972;34:484–9.
[36] Green RL, Cooper J, Smith EW. A unified theory of Stark broadening for hydrogenic ions—I: A general theory (including time ordering). J Quant Spectrosc Rad Transf. 1975;15:1025–36.
[37] Oks E. The shape of spectral lines of two-electron Rydberg atoms/ions: analytical solution. J Phys B: At Mol Opt Phys. 2017;50:115001.
[38] Wigner EP. Group theory. New York: Academic Press; 1964.
[39] Salzmann D. Atomic physics in hot plasmas. Oxford: Oxford Univ. Press; 1998.
[40] Griem HR. Spectral line broadening by plasmas. New York: Academic Press; 1974.
[41] Stambulchik E, Maron Y. Zeeman effect induced by intense laser light. Phys Rev Lett. 2014;113:083002.
[42] Sholin GV, Oks E. Theory of optical polarization measurements of turbulence spectrum in plasmas. Sov Phys Doklady. 1973;18:254–7.
[43] Oks E, Sholin GV. On Stark profiles of hydrogen lines in a plasma with low-frequency turbulence. Sov Phys Tech Phys. 1976;21:144–51.
[44] Swanson DG. Plasma waves. Bristol, UK: IOP Publishing; 2003.
[45] Tsytovich VN. An introduction to the theory of plasma turbulence. Oxford: Pergamon; 2016.
[46] Kadomtsev BB. Plasma turbulence. Cambridge: Academic Press; 1965.
[47] Stambulchik E. Stark broadening of Lyman-α in the presence of a strong magnetic field. Atoms. 2023;11:120.
[48] Bertschinger G, Messungen von VUV. Linien in einem dichten Z-Pinch-Plasma. Diss. Dokt. Bochum: Der Naturwissenschaften, Ruhr University; 1980.
[49] Alexiou S. Analysis of plasma emission experiments and 'dips'. Atoms. 2023;11:29.
[50] Zeldovich YaB. The quasienergy of a quantum-mechanical system subjected to a periodic action. Sov Phys JETP. 1967;24:1006–8.
[51] Ritus VI. Shift and splitting of atomic energy levels by the field of an electromagnetic wave. Sov Phys JETP. 1967;24:1041–4.
[52] Oks E, Dalimier E, Faenov AYa, Angelo P, Pikuz SA, Pikuz TA, et al. In-depth study of intra-Stark spectroscopy in the X-ray range in relativistic laser-plasma interactions. J Phys B: At Mol Opt Phys. 2017;50:245006.
[53] Zhuzhunashvili AI, Oks E. Technique of optical polarization measurements of plasma Langmuir turbulence spectrum. Sov Phys JETP. 1977;46:1122–9.
[54] Oks E, Rantsev-Kartinov VA. Spectroscopic observation and analysis of plasma turbulence in a Z-pinch. Sov Phys JETP. 1980;52:50–8.
[55] Jian L, Shali X, Qingguo Y, Lifeng L, Yufen W. Spatially-resolved spectra from a new uniform dispersion crystal spectrometer for characterization of Z-pinch plasmas. J Quant Spectrosc Rad Transf. 2013;116:41–8.
[56] Renner O, Dalimier E, Oks E, Krasniqi F, Dufour E, Schott R, et al. Experimental evidence of Langmuir-wave-caused features in spectral lines of laser-produced plasmas. J Quant Spectrosc Rad Transf. 2006;99:439–50.
[57] Oks E, Dalimier E, Faenov AY, Pikuz T, Fukuda Y, Jinno S, et al. Two-plasmon decay instability's signature in spectral lines and spectroscopic measurements of charge exchange rate in a femtosecond laser-driven cluster-based plasma. J Phys B: At Mol Opt Phys. 2014;47:221001.
[58] Oks E, Dalimier E, Faenov AY, Angelo P, Pikuz SA, Tubman E, et al. Using X-ray spectroscopy of relativistic laser plasma interaction to reveal parametric decay instabilities: a modeling tool for astrophysics. Opt Express. 2017;25:1958–72.
[59] Dalimier E, Faenov AY, Oks E, Angelo P, Pikuz TA, Fukuda Y, et al. X-ray spectroscopy of super intense laser-produced plasmas for

the study of nonlinear processes. Comparison with PIC simulations. J Phys Conf Ser. 2017;810:012004.
[60] Oks E. On the method of investigation of the mechanism of solar flares by hydrogen spectral lines. Sov Astron Lett. 1978;4:223–7.
[61] Gavrilenko VP. Resonance effects in the spectroscopy of atomic hydrogen in a plasma with a quasimonochromaticelectric field and located in a strong magnetic field. Sov Phys JETP. 1988;67:915–9.
[62] Blochinzew DI. Zur Theorie des Starkeffektes im Zeitveränderlichen Feld. Phys Z Sov Union. 1933;4:501–15.
[63] Oks E, Sholin GV. On influence of Langmuir noise anisotropy on Stark profiles of hydrogen spectral lines. Opt Spectrosc. 1977;42:434–6.
[64] Griem HR. Plasma Spectrosc. New York: McGraw-Hill; 1964.
[65] Günter S, Konies A. Influence of many-particle effects on spectral line shapes in nonthermal plasmas. Phys Rev E. 1994;49:4732–40.
[66] Fujimoto T, Iwamae A. Plasma polarization spectroscopy. Berlin: Springer; 2008.
[67] Ochkin VN. Spectroscopy of low temperature plasma. Weinheim, Germany: Wiley; 2009.
[68] Sobelman II, Vainshtein LA, Yukov EA. Excitation of atoms and broadening of spectral lines. Springer Ser Chem Phys. Vol. 7. Heidelberg: Springer; 1981.
[69] Sobelman II. Atomic spectra and radiative transitions. Springer Ser. Atoms Plasmas. Vol. 12, 2nd edn. Berlin: Springer; 1992.
[70] Baranger M. Simplified quantum-mechanical theory of pressure broadening. Phys Rev. 1958;111:481–93.
[71] Baranger M. Problem of overlapping lines in the theory of pressure broadening. Phys Rev. 1958;111:494–504.
[72] Kepple P, Griem HR. Improved Stark profile calculations for the hydrogen lines Hα, Hβ, Hγ, and Hδ. Phys Rev. 1968;173:317–25.
[73] Vidal CR, Cooper J, Smith EW. Hydrogen Stark broadening calculations with the unified classical path theory. J Quant Spectrosc Rad Transf. 1970;10:1011–63.
[74] Vidal CR, Cooper J, Smith EW. Unified theory calculations of Stark broadened hydrogen lines including lower state interactions. J Quant Spectrosc Rad Transf. 1971;11:263–81.
[75] Sholin GV, Lisitsa VS, Kogan VI. Amplitude modulation and bob-adiabaticity in the Stark broadening of hydrogen lines in plasmas. Sov Phys JETP. 1971;32:758–65.
[76] Büscher S, Wrubel T, Ferri S, Kunze H-J. The Stark width and shift of the hydrogen Hα line. J Phys B: At Mol Opt Phys. 2002;35(35):2889–97.
[77] Inglis DR, Teller E. Ionic depression of series limit in one-electron spectra. Astrophys J. 1939;90:439–48.
[78] Sholin GV. Stark broadening of hydrogen lines in a turbulent plasma. Sov Phys – Dokl. 1971;15:1040–3.
[79] Lisitsa VS, Jakovlenko SI. Optical and radiative collisions. Sov Phys – JETP. 1974;39:759–63.
[80] Lisitsa VS, Jakovlenko SI. A nonlinear theory of broadening and a generalization of the Karplus-Schwinger formula. Sov Phys – JETP. 1975;41:233–40.
[81] von Traubenberg HR, Gebauer R, Schrödinger E. Uber das Verhalten des Starkeffekts bei plötzlichen Feldänderungen. Z Phys. 1932;73:309–17.
[82] Lifshitz EV. Stark effect in high frequency stochastic fields in a plasma. Sov Phys – JETP. 1968;26:570–4.
[83] Tomashevsky IL. Fine structure of hydrogen-like atom quasienergy levels in a varying electric field. Spektroskopiya mnogozaryadnikh ionov [Spectroscopy of Multiply Charged Ions]. Moscow: USSR Acad Sci Scientific Council on Spectroscopy; 1986. p. 109 (in Russian).
[84] Lisitsa VS. Stark broadening of hydrogen lines in plasmas. Sov Phys – Usp. 1977;20:603–30.
[85] Sholin GV, Demura AV, Lisitsa VS. Theory of stark broadening of hydrogen lines in plasma. Sov Phys – JETP. 1973;37:1057–65.
[86] Demura AV, Sholin GV. Theory of asymmetry of Stark profiles of hydrogen spectral lines in dense plasmas. J Quant Spectrosc Rad Transf. 1975;15:881–99.
[87] Bacon ME. The asymmetry of Ly-α and Ly-β. J Quant Spectrosc Rad Transf. 1977;17:501–12.
[88] Demura AV, Demchenko GV, Nicolic D. Multiparametric dependence of hydrogen Stark profiles asymmetry. Eur Phys J D. 2008;45:111–27.
[89] Stehle C, Gilles D, Demura AV. Asymmetry of Stark profiles: the microfield point of view. Eur Phys J D. 2000;12:355–67.
[90] Demura AV. Beyond the linear Stark effect: A retrospective. Atoms. 2018;6:33.
[91] Demura AV, Gilles D, Stehle C. Asymmetry of Stark profiles in nonuniform fluctuating microfield. AIP Conf Proc. 2001;555:99–107
[92] Stehle C, Busquet M, Gilles D, Demura AV. On Stark broadening as a tool for diagnostics of high density plasmas. Laser Part Beams. 2005;23:357–63.
[93] Demura AV, Gilles D, Stehle C. Line asymmetries and plasma statistics. AIP Conf Proc. 1997;386:119–20.
[94] Demura AV, Demchenko GV, Nicolic D. On asymmetry of hydrogen spectral lines in nonequlibrium plasmas. AIP Conf Proc. 2008;851:46–8.
[95] Demura AV, Gilles D, Stehle C. Comparative study of microfield nonuniformity in plasmas. J Quant Spectr Rad Transf. 1995;54:123–36.
[96] Anufrienko AV, Bulyshev AE, Godunov AL, Demura AV, Zemtsov YUK, Lisitsa VS. Nonlinear interference effects and ion dynamics in the kinetic theory of Stark broadening of the spectral lines of multicharged ions in a dense plasma. JETP. 1993;76:219–28.
[97] Demura AV, Helbig W, Nicolic D. Asymmetry and shifts interdependence in Stark Profiles. AIP Conf Proc. 2002;645:318–24.
[98] Demura AV, Stehle C. On asymmetry in wings of Stark profiles. AIP Conf Proc. 2001;559:111–13.
[99] Volod'ko DA, Gavrilenko VP. Spectrum of a hydrogenlike atom in static magnetic and oscillating electric fields. Opt Spectrosc. 1988;64:155–8.
[100] Iglesias CA. Reformulation of plasma spectral line broadening with computer simulations. High Energy Density Phys. 2019;33:100707.
[101] Strekalov ML, Burshtein AI. Collapse of shock-broadened multiplets. Sov Phys JETP. 1972;34:53–8.
[102] Kim SH, Wilhelm HE. Stark effect and line broadening in three-dimensional stochastic fields. J Appl Phys. 1973;44:802–10.
[103] Cohn A, Bakshi R, Kalman G. Linear Stark effect due to resonant interactions of static and dynamic fields. Phys Rev Lett. 1972;29:324–7.
[104] Cohn A, Bakshi R, Kalman G. Corrigenda. Phys Rev Lett. 1973;31:620–0.
[105] Bakshi R, Kalman G, Cohn A. Hydrogenic Stark-Zeeman spectra for combined static and dynamic fields. Phys Rev Lett. 1973;31:1576–80.

[106] Rosato J, Marandet Y, Stamm R. A new table of Balmer line shapes for the diagnostic of magnetic fusion plasmas. J Quant Spectrosc Rad Transf. 2017;187:333–7.
[107] Rosato J, Kieu N, Hannachi I, Koubuti M, Marandet Y, Stamm R, et al. Stark-Zeeman line shape modeling for magnetic white dwarf and tokamak edge plasmas: common challenges. Atoms. 2017;5:36.
[108] Rosato J, Hannachi I, Marandet Y, Stamm R. Line shape models for magnetized hydrogen plasmas. J Phys Conf Ser. 2017;810:012011.
[109] Rosato J, Godbert-Mouret L, Koubiti M, Marandet Y, Stamm R. Stark broadening of hydrogen lines in magnetic fusion plasmas. AIP Conf Proc. 2017;1811:100001.
[110] Hannachi I, Meireni M, Rosato J, Stamm R, Marandet Y. Possible spectroscopic signature of wave collapse in edge plasmas. Contrib Plasma Phys. 2018;58:583–8.
[111] Rosato J, Kieu N, Meireni M, Hannachi I, Koubuti M, Marandet Y, et al. Stark broadening of Balmer lines with low and moderate quantum number in dense divertor plasmas. Contrib Plasma Phys. 2018;58:578–82.
[112] Meireni M, Hannachi I, Rosato J, Marandet Y, Stamm R. Spectroscopic models for the characterization of energetic particle beams in tokamak edge plasmas. Contrib Plasma Phys. 2018;58:589–93.
[113] Rosato J, Marandet Y, Reiter D, Stamm R. Design of a hybrid Monte Carlo method for line radiation transport simulations in magnetic fusion. J Comp Theor Transport. 2018;47:46–57.
[114] Sheeba RR, Koubuti M, Marandet Y, Qbaich T, Rosato J, Stamm R. Modeling of line and continuum spectral emission of hydrogen for recombining plasma conditions. J Phys Conf Ser. 2019;1289:012041.
[115] Stamm R, Hannachi I, Meireni M, Godbert-Mouret L, Koubuti M, Marandet Y, et al. Stark broadening from impact theory to simulations. Atoms. 2017;5:32.
[116] Meireni M, Hannachi I, Rosato J, Koubuti M, Marandet Y, Stamm R. Modeling of synthetic spectra in tokamak edge plasmas. J Phys Conf Ser. 2019;1289:012036.
[117] Hannachi I, Meireni M, Rosato J, Stamm R, Marandet Y. Effect of wave collapse on Lyman and Balmer lines. J Phys Conf Ser. 2019;1289:012034.
[118] Rosato J, Koubiti M, Marandet Y, Stamm R. Modeling of photon trapping effects in high-density divertor plasmas. J Quant Spectrosc Rad Transf. 2020;247:106949.
[119] Rosato J, Marandet Y, Stamm R. Quantifying the statistical noise in computer simulations of Stark broadening. J Quant Spectrosc Rad Transf. 2020;249:107002.
[120] Raji A, Rosato J, Stamm R, Marandet Y. New analysis of Balmer line shapes in magnetic white dwarf atmospheres. Eur Phys J D. 2021;75:63.